IOP Publishing Classical and Quantum Gravity

Class. Quantum Grav. **31** (2014) 165014 (27pp) doi:10.1088/0264-9381/31/16/165014

Implementation of an $\mathcal{F}$-statistic all-sky search for continuous gravitational waves in Virgo VSR1 data

J Aasi[1], B P Abbott[1], R Abbott[1], T Abbott[2], M R Abernathy[1], T Accadia[3], F Acernese[4,5], K Ackley[6], C Adams[7], T Adams[8], P Addesso[5], R X Adhikari[1], C Affeldt[9], M Agathos[10], N Aggarwal[11], O D Aguiar[12], A Ain[13], P Ajith[14], A Alemic[15], B Allen[9,16,17], A Allocca[18,19], D Amariutei[6], M Andersen[20], R Anderson[1], S B Anderson[1], W G Anderson[16], K Arai[1], M C Araya[1], C Arceneaux[21], J Areeda[22], S M Aston[7], P Astone[23], P Aufmuth[17], C Aulbert[9], L Austin[1], B E Aylott[24], S Babak[25], P T Baker[26], G Ballardin[27], S W Ballmer[15], J C Barayoga[1], M Barbet[6], B C Barish[1], D Barker[28], F Barone[4,5], B Barr[29], L Barsotti[11], M Barsuglia[30], M A Barton[28], I Bartos[31], R Bassiri[20], A Basti[18,32], J C Batch[28], J Bauchrowitz[9], Th S Bauer[10], B Behnke[25], M Bejger[33], M G Beker[10], C Belczynski[34], A S Bell[29], C Bell[29], G Bergmann[9], D Bersanetti[35,36], A Bertolini[10], J Betzwieser[7], P T Beyersdorf[37], I A Bilenko[38], G Billingsley[1], J Birch[7], S Biscans[11], M Bitossi[18], M A Bizouard[39], E Black[1], J K Blackburn[1], L Blackburn[40], D Blair[41], S Bloemen[42,10], M Blom[10], O Bock[9], T P Bodiya[11], M Boer[43], G Bogaert[43], C Bogan[9], C Bond[24], F Bondu[44], L Bonelli[18,32], R Bonnand[45], R Bork[1], M Born[9], K Borkowski[46], V Boschi[18], Sukanta Bose[47,13], L Bosi[48], C Bradaschia[18], P R Brady[16], V B Braginsky[38], M Branchesi[49,50], J E Brau[51], T Briant[52], D O Bridges[7], A Brillet[43], M Brinkmann[9], V Brisson[39], A F Brooks[1], D A Brown[15], D D Brown[24], F Brückner[24], S Buchman[20], T Bulik[34], H J Bulten[10,53], A Buonanno[54], R Burman[41], D Buskulic[3], C Buy[30], L Cadonati[55], G Cagnoli[45], J Calderón Bustillo[56], E Calloni[4,57], J B Camp[40], P Campsie[29], K C Cannon[58], B Canuel[27], J Cao[59], C D Capano[54], F Carbognani[27], L Carbone[24], S Caride[60], A Castiglia[61], S Caudill[16], F Cavalier[39], R Cavalieri[27], C Celerier[20], G Cella[18], C Cepeda[1], E Cesarini[62], R Chakraborty[1], T Chalermsongsak[1], S J Chamberlin[16], S Chao[63], P Charlton[64], E Chassande Mottin[30], X Chen[41], Y Chen[65],

A Chincarini[35], A Chiummo[27], H S Cho[66], J Chow[67], N Christensen[68], Q Chu[41], S S Y Chua[67], S Chung[41], G Ciani[6], F Clara[28], J A Clark[55], F Cleva[43], E Coccia[69,70], P F Cohadon[52], A Colla[23,71], C Collette[72], M Colombini[48], L Cominsky[73], A Conte[23,71], D Cook[28], T R Corbitt[2], M Cordier[37], N Cornish[26], A Corpuz[74], A Corsi[75], C A Costa[12], M W Coughlin[76], S Coughlin[77], J P Coulon[43], S Countryman[31], P Couvares[15], D M Coward[41], M Cowart[7], D C Coyne[1], R Coyne[75], K Craig[29], J D E Creighton[16], S G Crowder[78], A Cumming[29], L Cunningham[29], E Cuoco[27], K Dahl[9], T Dal Canton[9], M Damjanic[9], S L Danilishin[41], S D'Antonio[62], K Danzmann[9,17], V Dattilo[27], H Daveloza[79], M Davier[39], G S Davies[29], E J Daw[80], R Day[27], T Dayanga[47], G Debreczeni[81], J Degallaix[45], S Deléglise[52], W Del Pozzo[10], T Denker[9], T Dent[9], H Dereli[43], V Dergachev[1], R De Rosa[4,57], R T DeRosa[2], R DeSalvo[82], S Dhurandhar[13], M Díaz[79], L Di Fiore[4], A Di Lieto[18,32], I Di Palma[9], A Di Virgilio[18], A Donath[25], F Donovan[11], K L Dooley[9], S Doravari[7], O Dorosh[83], S Dossa[68], R Douglas[29], T P Downes[16], M Drago[84,85], R W P Drever[1], J C Driggers[1], Z Du[59], S Dwyer[28], T Eberle[9], T Edo[80], M Edwards[8], A Effler[2], H Eggenstein[9], P Ehrens[1], J Eichholz[6], S S Eikenberry[6], G Endrőczi[81], R Essick[11], T Etzel[1], M Evans[11], T Evans[7], M Factourovich[31], V Fafone[62,70], S Fairhurst[8], Q Fang[41], S Farinon[35], B Farr[77], W M Farr[24], M Favata[86], H Fehrmann[9], M M Fejer[20], D Feldbaum[6,7], F Feroz[76], I Ferrante[18,32], F Ferrini[27], F Fidecaro[18,32], L S Finn[87], I Fiori[27], R P Fisher[15], R Flaminio[45], J D Fournier[43], S Franco[39], S Frasca[23,71], F Frasconi[18], M Frede[9], Z Frei[88], A Freise[24], R Frey[51], T T Fricke[9], P Fritschel[11], V V Frolov[7], P Fulda[6], M Fyffe[7], J Gair[76], L Gammaitoni[48,89], S Gaonkar[13], F Garufi[4,57], N Gehrels[40], G Gemme[35], E Genin[27], A Gennai[18], S Ghosh[10,42,47], J A Giaime[7,2], K D Giardina[7], A Giazotto[18], C Gill[29], J Gleason[6], E Goetz[9], R Goetz[6], L Gondan[88], G González[2], N Gordon[29], M L Gorodetsky[38], S Gossan[65], S Goßler[9], R Gouaty[3], C Gräf[29], P B Graff[40], M Granata[45], A Grant[29], S Gras[11], C Gray[28], R J S Greenhalgh[90], A M Gretarsson[74], P Groot[42], H Grote[9], K Grover[24], S Grunewald[25], G M Guidi[49,50], C Guido[7], K Gushwa[1], E K Gustafson[1], R Gustafson[60], D Hammer[16], G Hammond[29], M Hanke[9], J Hanks[28], C Hanna[91], J Hanson[7], J Harms[1], G M Harry[92], I W Harry[15], E D Harstad[51], M Hart[29], M T Hartman[6], C J Haster[24], K Haughian[29], A Heidmann[52], M Heintze[6,7], H Heitmann[43], P Hello[39], G Hemming[27], M Hendry[29], I S Heng[29], A W Heptonstall[1], M Heurs[9],

M Hewitson[9], S Hild[29], D Hoak[55], K A Hodge[1], K Holt[7], S Hooper[41], P Hopkins[8], D J Hosken[93], J Hough[29], E J Howell[41], Y Hu[29], E Huerta[15], B Hughey[74], S Husa[56], S H Huttner[29], M Huynh[16], T Huynh Dinh[7], D R Ingram[28], R Inta[87], T Isogai[11], A Ivanov[1], B R Iyer[94], K Izumi[28], M Jacobson[1], E James[1], H Jang[95], P Jaranowski[96], Y Ji[59], F Jiménez Forteza[56], W W Johnson[2], D I Jones[97], R Jones[29], R J G Jonker[10], L Ju[41], Haris K[98], P Kalmus[1], V Kalogera[77], S Kandhasamy[21], G Kang[95], J B Kanner[1], J Karlen[55], M Kasprzack[27,39], E Katsavounidis[11], W Katzman[7], H Kaufer[17], K Kawabe[28], F Kawazoe[9], F Kéfélian[43], G M Keiser[20], D Keitel[9], D B Kelley[15], W Kells[1], A Khalaidovski[9], F Y Khalili[38], E A Khazanov[99], C Kim[95,100], K Kim[101], N Kim[20], N G Kim[95], Y M Kim[66], E J King[93], P J King[1], D L Kinzel[7], J S Kissel[28], S Klimenko[6], J Kline[16], S Koehlenbeck[9], K Kokeyama[2], V Kondrashov[1], S Koranda[16], W Z Korth[1], I Kowalska[34], D B Kozak[1], A Kremin[78], V Kringel[9], B Krishnan[9], A Królak[83,102], G Kuehn[9], A Kumar[103], P Kumar[15], R Kumar[29], L Kuo[63], A Kutynia[83], P Kwee[11], M Landry[28], B Lantz[20], S Larson[77], P D Lasky[104], C Lawrie[29], A Lazzarini[1], C Lazzaro[105], P Leaci[25], S Leavey[29], E O Lebigot[59], C H Lee[66], H K Lee[101], H M Lee[100], J Lee[11], M Leonardi[84,85], J R Leong[9], A Le Roux[7], N Leroy[39], N Letendre[3], Y Levin[106], B Levine[28], J Lewis[1], T G F Li[1,10], K Libbrecht[1], A Libson[11], A C Lin[20], T B Littenberg[77], V Litvine[1], N A Lockerbie[107], V Lockett[22], D Lodhia[24], K Loew[74], J Logue[29], A L Lombardi[55], M Lorenzini[62,70], V Loriette[108], M Lormand[7], G Losurdo[49], J Lough[15], M J Lubinski[28], H Lück[9,17], E Luijten[77], A P Lundgren[9], R Lynch[11], Y Ma[41], J Macarthur[29], E P Macdonald[8], T MacDonald[20], B Machenschalk[9], M MacInnis[11], D M Macleod[2], F Magana Sandoval[15], M Mageswaran[1], C Maglione[109], K Mailand[1], E Majorana[23], I Maksimovic[108], V Malvezzi[62,70], N Man[43], G M Manca[9], I Mandel[24], V Mandic[78], V Mangano[23,71], N Mangini[55], M Mantovani[18], F Marchesoni[48,110], F Marion[3], S Márka[31], Z Márka[31], A Markosyan[20], E Maros[1], J Marque[27], F Martelli[49,50], I W Martin[29], R M Martin[6], L Martinelli[43], D Martynov[1], J N Marx[1], K Mason[11], A Masserot[3], T J Massinger[15], F Matichard[11], L Matone[31], R A Matzner[111], N Mavalvala[11], N Mazumder[98], G Mazzolo[9,17], R McCarthy[28], D E McClelland[67], S C McGuire[112], G McIntyre[1], J McIver[55], K McLin[73], D Meacher[43], G D Meadors[60], M Mehmet[9], J Meidam[10], M Meinders[17], A Melatos[104], G Mendell[28], R A Mercer[16], S Meshkov[1], C Messenger[29], P Meyers[78],

H Miao[65], C Michel[45], E E Mikhailov[113], L Milano[4,57], S Milde[25], J Miller[11], Y Minenkov[62], C M F Mingarelli[24], C Mishra[98], S Mitra[13], V P Mitrofanov[38], G Mitselmakher[6], R Mittleman[11], B Moe[16], P Moesta[65], M Mohan[27], S R P Mohapatra[15,61], D Moraru[28], G Moreno[28], N Morgado[45], S R Morriss[79], K Mossavi[9], B Mours[3], C M Mow Lowry[9], C L Mueller[6], G Mueller[6], S Mukherjee[79], A Mullavey[2], J Munch[93], D Murphy[31], P G Murray[29], A Mytidis[6], M F Nagy[81], D Nanda Kumar[6], I Nardecchia[62,70], L Naticchioni[23,71], R K Nayak[114], V Necula[6], G Nelemans[42,10], I Neri[48,89], M Neri[35,36], G Newton[29], T Nguyen[67], A Nitz[15], F Nocera[27], D Nolting[7], M E N Normandin[79], L K Nuttall[16], E Ochsner[16], J O'Dell[90], E Oelker[11], J J Oh[115], S H Oh[115], F Ohme[8], P Oppermann[9], B O'Reilly[7], R O'Shaughnessy[16], C Osthelder[1], D J Ottaway[93], R S Ottens[6], H Overmier[7], B J Owen[87], C Padilla[22], A Pai[98], O Palashov[99], C Palomba[23], H Pan[63], Y Pan[54], C Pankow[16], F Paoletti[18,27], R Paoletti[18,19], M A Papa[16,25], H Paris[28], A Pasqualetti[27], R Passaquieti[18,32], D Passuello[18], M Pedraza[1], S Penn[116], A Perreca[15], M Phelps[1], M Pichot[43], M Pickenpack[9], F Piergiovanni[49,50], V Pierro[35,82], M Pietka[117], L Pinard[45], I M Pinto[35,82], M Pitkin[29], J Poeld[9], R Poggiani[18,32], A Poteomkin[99], J Powell[29], J Prasad[13], S Premachandra[106], T Prestegard[78], L R Price[1], M Prijatelj[27], S Privitera[1], G A Prodi[84,85], L Prokhorov[38], O Puncken[79], M Punturo[48], P Puppo[23], J Qin[41], V Quetschke[79], E Quintero[1], G Quiroga[109], R Quitzow James[51], F J Raab[28], D S Rabeling[10,53], I Rácz[81], H Radkins[28], P Raffai[88], S Raja[118], G Rajalakshmi[14], M Rakhmanov[79], C Ramet[7], K Ramirez[79], P Rapagnani[23,71], V Raymond[1], V Re[62,70], J Read[22], C M Reed[28], T Regimbau[43], S Reid[119], D H Reitze[1,6], E Rhoades[74], F Ricci[23,71], K Riles[60], N A Robertson[1,29], F Robinet[39], A Rocchi[62], M Rodruck[28], L Rolland[3], J G Rollins[1], R Romano[4,5], G Romanov[113], J H Romie[7], D Rosińska[33,120], S Rowan[29], A Rüdiger[9], P Ruggi[27], K Ryan[28], F Salemi[9], L Sammut[104], V Sandberg[28], J R Sanders[60], V Sannibale[1], I Santiago Prieto[29], E Saracco[45], B Sassolas[45], B S Sathyaprakash[8], P R Saulson[15], R Savage[28], J Scheuer[77], R Schilling[9], R Schnabel[9,17], R M S Schofield[51], E Schreiber[9], D Schuette[9], B F Schutz[8,25], J Scott[29], S M Scott[67], D Sellers[7], A S Sengupta[121], D Sentenac[27], V Sequino[62,70], A Sergeev[99], D Shaddock[67], S Shah[10,42], M S Shahriar[77], M Shaltev[9], B Shapiro[20], P Shawhan[54], D H Shoemaker[11], T L Sidery[24], K Siellez[43], X Siemens[16], D Sigg[28], D Simakov[9], A Singer[1], L Singer[1], R Singh[2], A M Sintes[56], B J J Slagmolen[67], J Slutsky[9],

J R Smith[22], M Smith[1], R J E Smith[1], N D Smith Lefebvre[1], E J Son[115], B Sorazu[29], T Souradeep[13], L Sperandio[62,70], A Staley[31], J Stebbins[20], J Steinlechner[9], S Steinlechner[9], B C Stephens[16], S Steplewski[47], S Stevenson[24], R Stone[79], D Stops[24], K A Strain[29], N Straniero[45], S Strigin[38], R Sturani[49,50,122], A L Stuver[7], T Z Summerscales[123], S Susmithan[41], P J Sutton[8], B Swinkels[27], M Tacca[30], D Talukder[51], D B Tanner[6], S P Tarabrin[9], R Taylor[1], A P M ter Braack[10], M P Thirugnanasambandam[1], M Thomas[7], P Thomas[28], K A Thorne[7], K S Thorne[65], E Thrane[1], V Tiwari[6], K V Tokmakov[107], C Tomlinson[80], A Toncelli[18,32], M Tonelli[18,32], O Torre[18,19], C V Torres[79], C I Torrie[1,29], F Travasso[48,89], G Traylor[7], M Tse[11,31], D Ugolini[124], C S Unnikrishnan[14], A L Urban[16], K Urbanek[20], H Vahlbruch[17], G Vajente[18,32], G Valdes[79], M Vallisneri[65], J F J vanden Brand[10,53], C VanDen Broeck[10], S vander Putten[10], M V vander Sluys[10,42], J van Heijningen[10], A A van Veggel[29], S Vass[1], M Vasúth[81], R Vaulin[11], A Vecchio[24], G Vedovato[105], J Veitch[10], P J Veitch[93], K Venkateswara[125], D Verkindt[3], S S Verma[41], F Vetrano[49,50], A Viceré[49,50], R Vincent Finley[112], J Y Vinet[43], S Vitale[11], T Vo[28], H Vocca[48,89], C Vorvick[28], W D Vousden[24], S P Vyachanin[38], A Wade[67], L Wade[16], M Wade[16], M Walker[2], L Wallace[1], M Wang[24], X Wang[59], R L Ward[67], M Was[9], B Weaver[28], L W Wei[43], M Weinert[9], A J Weinstein[1], R Weiss[11], T Welborn[7], L Wen[41], P Wessels[9], M West[15], T Westphal[9], K Wette[9], J T Whelan[61], D J White[80], B F Whiting[6], K Wiesner[9], C Wilkinson[28], K Williams[112], L Williams[6], R Williams[1], T Williams[126], A R Williamson[8], J L Willis[127], B Willke[17,9], M Wimmer[9], W Winkler[9], C C Wipf[11], A G Wiseman[16], H Wittel[9], G Woan[29], J Worden[28], J Yablon[77], I Yakushin[7], H Yamamoto[1], C C Yancey[54], H Yang[65], Z Yang[59], S Yoshida[126], M Yvert[3], A Zadrożny[83], M Zanolin[74], J P Zendri[105], Fan Zhang[11,59], L Zhang[1], C Zhao[41], X J Zhu[41], M E Zucker[11], S Zuraw[55] and J Zweizig[1]

[1] LIGO—California Institute of Technology, Pasadena, CA 91125, USA
[2] Louisiana State University, Baton Rouge, LA 70803, USA
[3] Laboratoire d'Annecy-le-Vieux de Physique des Particules (LAPP), Université de Savoie, CNRS/IN2P3, F-74941 Annecy-le-Vieux, France
[4] INFN, Sezione di Napoli, Complesso Universitario di Monte S.Angelo, I-80126 Napoli, Italy
[5] Università di Salerno, Fisciano, I-84084 Salerno, Italy
[6] University of Florida, Gainesville, FL 32611, USA
[7] LIGO—Livingston Observatory, Livingston, LA 70754, USA
[8] Cardiff University, Cardiff, CF24 3AA, UK

[9] Albert-Einstein-Institut, Max-Planck-Institut für Gravitationsphysik, D-30167 Hannover, Germany
[10] Nikhef, Science Park, 1098 XG Amsterdam, The Netherlands
[11] LIGO—Massachusetts Institute of Technology, Cambridge, MA 02139, USA
[12] Instituto Nacional de Pesquisas Espaciais, 12227-010—São José dos Campos, SP, Brazil
[13] Inter-University Centre for Astronomy and Astrophysics, Pune—411007, India
[14] Tata Institute for Fundamental Research, Mumbai 400005, India
[15] Syracuse University, Syracuse, NY 13244, USA
[16] University of Wisconsin–Milwaukee, Milwaukee, WI 53201, USA
[17] Leibniz Universität Hannover, D-30167 Hannover, Germany
[18] INFN, Sezione di Pisa, I-56127 Pisa, Italy
[19] Università di Siena, I-53100 Siena, Italy
[20] Stanford University, Stanford, CA 94305, USA
[21] The University of Mississippi, University, MS 38677, USA
[22] California State University Fullerton, Fullerton, CA 92831, USA
[23] INFN, Sezione di Roma, I-00185 Roma, Italy
[24] University of Birmingham, Birmingham B15 2TT, UK
[25] Albert-Einstein-Institut, Max-Planck-Institut für Gravitationsphysik, D-14476 Golm, Germany
[26] Montana State University, Bozeman, MT 59717, USA
[27] European Gravitational Observatory (EGO), I-56021 Cascina, Pisa, Italy
[28] LIGO—Hanford Observatory, Richland, WA 99352, USA
[29] SUPA, University of Glasgow, Glasgow G12 8QQ, UK
[30] APC, AstroParticule et Cosmologie, Université Paris Diderot, CNRS/IN2P3, CEA/Irfu, Observatoire de Paris, Sorbonne Paris Cité, 10, rue Alice Domon et Léonie Duquet, F-75205 Paris Cedex 13, France
[31] Columbia University, New York, NY 10027, USA
[32] Università di Pisa, I-56127 Pisa, Italy
[33] CAMK-PAN, 00-716 Warsaw, Poland
[34] Astronomical Observatory Warsaw University, 00-478 Warsaw, Poland
[35] INFN, Sezione di Genova, I-16146 Genova, Italy
[36] Università degli Studi di Genova, I-16146 Genova, Italy
[37] San Jose State University, San Jose, CA 95192, USA
[38] Faculty of Physics, Lomonosov Moscow State University, Moscow 119991, Russia
[39] LAL, Université Paris-Sud, IN2P3/CNRS, F-91898 Orsay, France
[40] NASA/Goddard Space Flight Center, Greenbelt, MD 20771, USA
[41] University of Western Australia, Crawley, WA 6009, Australia
[42] Department of Astrophysics/IMAPP, Radboud University Nijmegen, PO Box 9010, 6500 GL Nijmegen, The Netherlands
[43] Université Nice-Sophia-Antipolis, CNRS, Observatoire de la Côte d'Azur, F-06304 Nice, France
[44] Institut de Physique de Rennes, CNRS, Université de Rennes 1, F-35042 Rennes, France
[45] Laboratoire des Matériaux Avancés (LMA), IN2P3/CNRS, Université de Lyon, F-69622 Villeurbanne, Lyon, France
[46] Centre for Astronomy, Nicolaus Copernicus University, 87-100 Toruń, Poland
[47] Washington State University, Pullman, WA 99164, USA
[48] INFN, Sezione di Perugia, I-06123 Perugia, Italy
[49] INFN, Sezione di Firenze, I-50019 Sesto Fiorentino, Firenze, Italy
[50] Università degli Studi di Urbino 'Carlo Bo', I-61029 Urbino, Italy
[51] University of Oregon, Eugene, OR 97403, USA

[52] Laboratoire Kastler Brossel, ENS, CNRS, UPMC, Université Pierre et Marie Curie, F-75005 Paris, France
[53] VU University Amsterdam, 1081 HV Amsterdam, The Netherlands
[54] University of Maryland, College Park, MD 20742, USA
[55] University of Massachusetts—Amherst, Amherst, MA 01003, USA
[56] Universitat de les Illes Balears, E-07122 Palma de Mallorca, Spain
[57] Università di Napoli 'Federico II', Complesso Universitario di Monte S.Angelo, I-80126 Napoli, Italy
[58] Canadian Institute for Theoretical Astrophysics, University of Toronto, Toronto, Ontario M5S 3H8, Canada
[59] Tsinghua University, Beijing 100084, People's Republic of China
[60] University of Michigan, Ann Arbor, MI 48109, USA
[61] Rochester Institute of Technology, Rochester, NY 14623, USA
[62] INFN, Sezione di Roma Tor Vergata, I-00133 Roma, Italy
[63] National Tsing Hua University, Hsinchu, Taiwan 300
[64] Charles Sturt University, Wagga Wagga, NSW 2678, Australia
[65] Caltech-CaRT, Pasadena, CA 91125, USA
[66] Pusan National University, Busan 609-735, Korea
[67] Australian National University, Canberra, ACT 0200, Australia
[68] Carleton College, Northfield, MN 55057, USA
[69] INFN, Gran Sasso Science Institute, I-67100 L'Aquila, Italy
[70] Università di Roma Tor Vergata, I-00133 Roma, Italy
[71] Università di Roma 'La Sapienza', I-00185 Roma, Italy
[72] University of Brussels, Brussels 1050 Belgium
[73] Sonoma State University, Rohnert Park, CA 94928, USA
[74] Embry-Riddle Aeronautical University, Prescott, AZ 86301, USA
[75] The George Washington University, Washington DC 20052, USA
[76] University of Cambridge, Cambridge CB2 1TN, UK
[77] Northwestern University, Evanston, IL 60208, USA
[78] University of Minnesota, Minneapolis, MN 55455, USA
[79] The University of Texas at Brownsville, Brownsville, TX 78520, USA
[80] The University of Sheffield, Sheffield S10 2TN, UK
[81] Wigner RCP, RMKI, H-1121 Budapest, Konkoly Thege Miklósút 29-33, Hungary
[82] University of Sannio at Benevento, I-82100 Benevento, Italy
[83] NCBJ, 05-400Świerk-Otwock, Poland
[84] INFN, Gruppo Collegato di Trento, I-38050 Povo, Trento, Italy
[85] Università di Trento, I-38050 Povo, Trento, Italy
[86] Montclair State University, Montclair, NJ 07043, USA
[87] The Pennsylvania State University, University Park, PA 16802, USA
[88] MTA Eötvös University, 'Lendulet' ARG, Budapest 1117, Hungary
[89] Università di Perugia, I-06123 Perugia, Italy
[90] Rutherford Appleton Laboratory, HSIC, Chilton, Didcot, Oxon OX11 0QX, UK
[91] Perimeter Institute for Theoretical Physics, Waterloo, Ontario N2L 2Y5, Canada
[92] American University, Washington, DC 20016, USA
[93] University of Adelaide, Adelaide, SA 5005, Australia
[94] Raman Research Institute, Bangalore, Karnataka 560080, India
[95] Korea Institute of Science and Technology Information, Daejeon 305-806, Korea
[96] Białystok University, 15-424 Białystok, Poland
[97] University of Southampton, Southampton SO17 1BJ, UK
[98] IISER-TVM, CET Campus, Trivandrum Kerala 695016, India
[99] Institute of Applied Physics, Nizhny Novgorod, 603950, Russia
[100] Seoul National University, Seoul 151-742, Korea
[101] Hanyang University, Seoul 133-791, Korea

[102] IM-PAN, 00-956 Warsaw, Poland
[103] Institute for Plasma Research, Bhat, Gandhinagar 382428, India
[104] The University of Melbourne, Parkville, VIC 3010, Australia
[105] INFN, Sezione di Padova, I-35131 Padova, Italy
[106] Monash University, Victoria 3800, Australia
[107] SUPA, University of Strathclyde, Glasgow, G1 1XQ, UK
[108] ESPCI, CNRS, F-75005 Paris, France
[109] Argentinian Gravitational Wave Group, Cordoba Cordoba 5000, Argentina
[110] Università di Camerino, Dipartimento di Fisica, I-62032 Camerino, Italy
[111] The University of Texas at Austin, Austin, TX 78712, USA
[112] Southern University and A&M College, Baton Rouge, LA 70813, USA
[113] College of William and Mary, Williamsburg, VA 23187, USA
[114] IISER-Kolkata, Mohanpur, West Bengal 741252, India
[115] National Institute for Mathematical Sciences, Daejeon 305-390, Korea
[116] Hobart and William Smith Colleges, Geneva, NY 14456, USA
[117] Gjøvik videregående skole, Pb 534, NO-2803 Gjøvik, Norway
[118] RRCAT, Indore MP 452013, India
[119] SUPA, University of the West of Scotland, Paisley, PA1 2BE, UK
[120] Institute of Astronomy, 65-265 Zielona Góra, Poland
[121] Indian Institute of Technology, Gandhinagar Ahmedabad Gujarat 382424, India
[122] Instituto de Física Teórica, Univ. Estadual Paulista/International Center for Theoretical Physics—South American Institue for Research, São Paulo SP 01140-070, Brazil
[123] Andrews University, Berrien Springs, MI 49104, USA
[124] Trinity University, San Antonio, TX 78212, USA
[125] University of Washington, Seattle, WA 98195, USA
[126] Southeastern Louisiana University, Hammond, LA 70402, USA
[127] Abilene Christian University, Abilene, TX 79699, USA

Received 7 March 2014, revised 16 June 2014
Accepted for publication 2 July 2014
Published 5 August 2014

Abstract

We present an implementation of the $\mathcal{F}$-statistic to carry out the first search in data from the Virgo laser interferometric gravitational wave detector for periodic gravitational waves from *a priori* unknown, isolated rotating neutron stars. We searched a frequency f_0 range from 100 Hz to 1 kHz and the frequency dependent spindown f_1 range from $-1.6(f_0/100\,\mathrm{Hz}) \times 10^{-9}\,\mathrm{Hz\,s^{-1}}$ to zero. A large part of this frequency–spindown space was unexplored by any of the all-sky searches published so far. Our method consisted of a coherent search over two-day periods using the $\mathcal{F}$-statistic, followed by a search for coincidences among the candidates from the two-day segments. We have introduced a number of novel techniques and algorithms that allow the use of the fast Fourier transform (FFT) algorithm in the coherent part of the search resulting in a fifty-fold speed-up in computation of the $\mathcal{F}$-statistic with respect to the algorithm used in the other pipelines. No significant gravitational wave signal was found. The sensitivity of the search was estimated by injecting signals into the data. In the most sensitive parts of the detector band more than 90% of signals would have been detected with dimensionless gravitational-wave amplitude greater than 5×10^{-24}.

Keywords: gravitational waves, gravitational radiation detectors, pulsars, data analysis: algorithms and implementation
PACS numbers: 04.80.Nn, 95.55.Ym, 97.60.Gb, 07.05.Kf

(Some figures may appear in colour only in the online journal)

1. Introduction

This paper presents results from a wide parameter search for periodic gravitational waves from spinning neutron stars using data from the Virgo detector [1]. The data used in this paper were produced during Virgo's first science run (VSR1), which started on 18 May 2007 and ended on 1 October 2007. The VSR1 data have never been searched for periodic gravitational waves from isolated neutron stars before. The innovation of the search is the combination of the efficiency of the FFT algorithm together with a nearly optimal grid of templates.

Rotating neutron stars are promising sources of gravitational radiation in the band of ground-based laser interferometric detectors (see [2] for a review). In order for these objects to emit gravitational waves, they must exhibit some asymmetry, which could be due to imperfections of the neutron star crust or the influence of strong internal magnetic fields (see [3] for recent results). Gravitational radiation also may arise due to the r-modes, i.e., rotation-dominated oscillations driven unstable by the gravitational emission (see [4] for discussion of implications of r-modes for GW searches). Neutron star precession is another gravitational wave emission mechanism (see [5] for a recent study). Details of the above mechanisms of gravitational wave emission can be found in [6–11].

A signal from a rotating neutron star can be modeled independently of the specific mechanism of gravitational wave emission as a nearly periodic wave the frequency of which decreases slowly during the observation time due to the rotational energy loss. The signal registered by an Earth-based detector is both amplitude and phase modulated because of the motion of the Earth with respect to the source.

The gravitational wave signal from such a star is expected to be very weak, and therefore months-long segments of data must be analyzed. Assuming the moment of inertia $I = 10^{45}$ g cm^2, the maximum deformation that a neutron star can sustain, measured by the ellipticity parameter ϵ (equation (7)), ranges from 10^{-5} for ordinary matter, 10^{-3} for hybrid stars to 10^{-1} for color-superconducting quark stars (see [11] for details). For unknown neutron stars one needs to search a very large parameter space. As a result, fully coherent, blind searches are computationally prohibitive. To perform a fully coherent search of VSR1 data in real time (i.e., in the time of 136 days of duration of the VSR1 run) over the parameter space proposed in this paper would require a 1.4×10^4 petaflop computer [12].

A natural way to reduce the computational burden is a hierarchical scheme, where first short segments of data are analyzed coherently, and then results are combined incoherently. This leads to computationally manageable searches at the expense of the signal-to-ratio loss. To perform the hierarchical search presented in this paper in real time a 2.8 teraflop computer is required. One approach is to use short segments of the order of half an hour long so that the signal remains within a single Fourier frequency bin in each segment and thus a single Fourier transform suffices to extract the whole power of the gravitational wave signal in each segment. Three schemes were developed for the analysis of Fourier transforms of the short data segments and they were used in the all-sky searches of ground interferometer data: the 'stack-slide' [13], the 'Hough transform' [13, 14] and the 'PowerFlux' methods [13, 15, 16].

Another hierarchical scheme involves using longer segment duration for which signal modulations need to be taken into account. For segments of the order of days long, coherent analysis using the popular $\mathcal{F}$-statistic [17] is computationally demanding, but feasible. For example, the hierarchical search of VSR1 data presented in this paper requires around 1900 processor cores for the time of 136 days, which was the duration of the VSR1 run. In the hierarchical scheme the first coherent analysis step is followed by a post-processing step where data obtained in the first step are combined incoherently. This scheme was implemented by the distributed volunteer computing project Einstein@Home [18]. The E@H project performed analysis of LIGO S4 and S5 data, leading to results published in three papers. In the first two, [19, 20], the candidate signals from the coherent analysis were searched for coincidences. In the third paper [21] the results from the coherent search were analyzed using a Hough-transform scheme.

The search method used here is similar to the one used in the first two E@H searches: it consists of coherent analysis by means of the $\mathcal{F}$-statistic, followed by a search for coincidences among the candidates obtained in the coherent analysis. There are, however, important differences: in this search we have a fixed threshold for the coherent analysis, resulting in a variable number of candidates from analysis of each of the data segments. Moreover, for different bands we have a variable number of two-day data segments (see section 3 for details). In E@H searches the number of candidates used in coincidences from each data segment was the same, as was the number of data segments for each band. In addition, the duration of data segments for coherent analysis in the two first E@H searches was 30 h (48 h in this case).

In this analysis we have implemented algorithms and techniques that considerably improve the efficiency of this search. Most importantly we have used the FFT algorithm to evaluate the $\mathcal{F}$-statistic for two-day data segments. Also we were able to use the FFT algorithm together with a grid of templates that was only 20% denser than the best known grid (i.e., the one with the least number of points).

Given that the data we analyzed (Virgo VSR1) had higher noise and the duration was shorter than the LIGO S5 data we have achieved a lower sensitivity than in the most recent E@H search [21]. However, due to very good efficiency of our code we were able to analyze a much larger parameter space. We have analyzed a large part of the f–$\dot{f}$ plane that was previously unexplored by any of the all-sky searches. For example in this analysis the f–$\dot{f}$ plane searched was 6.5 larger than that in the full S5 E@H search [21] (see figure 5). In addition, the data from the Virgo detector are characterized by different spectral artifacts (instrumental and environmental) from these seen in LIGO data. As a result, certain narrow bands excluded from LIGO searches because of highly non-Gaussian noise can be explored in this analysis.

The paper is organized as follows. In section 2 we describe the data from the Virgo detector VSR1 run, in section 3 we explain how the data were selected. In section 4 the response of the detector to a gravitational wave signal from a rotating neutron star is briefly recalled. In section 5 we introduce the $\mathcal{F}$-statistic. In section 6 we describe the search method and present the algorithms for an efficient calculation of the $\mathcal{F}$-statistic. In section 7 we describe the vetoing procedure of the candidates. In section 8 we present the coincidence algorithm that is used for post-processing of the candidates. Section 9 contains results of the analysis. In section 10 we determine the sensitivity of this search, and we conclude the paper by section 11. In the appendix we present a general formula for probability that is used in the estimation of significance of the coincidences.

2. Data from the Virgo's first science run

The VSR1 science run spanned more than four months of data acquisition. This run started on 18 May 2007 at 21:00 UTC and ended on 1 October 2007 at 05:00 UTC. The detector was running close to its design sensitivity with a duty cycle of 81.0% [22]. The data were calibrated, and the time series of the gravitational wave strain $h(t)$ was reconstructed. In the range of frequencies from 10 Hz to 10 kHz the systematic error in amplitude was 6% and the phase error was 70 mrad below the frequency of 1.9 kHz [23]. A snapshot of the amplitude spectral density of VSR1 data in the Virgo detector band is presented in figure 1.

3. Data selection

The analysis input consists of narrow-band time-domain data segments. In order to obtain these sequences from VSR1 data, we have used the software described in [24], and extracted the segments from the Short Fourier Transform Database (SFDB). The time domain data sequences were extracted with a certain sampling time Δt, time duration $T_{\rm obs}$ and offset frequency $f_{\rm off}$. Thus each time domain sequence has the band $[f_{\rm off}, f_{\rm off} + B]$, where $B = 1/2 \times 1/\Delta t$. We choose the segment duration to be exactly two sidereal days and the sampling time equal to 1/2 s, i.e., the bandwidth $B = 1$ Hz. As a result each narrow band time segment contains $N = 344\,656$ data points. We have considered 67 two-day time frames for the analysis. The starting time of the analysis (the time of the first sample of the data in the first time frame) was 19 May 2007 at 00:00 UTC. The data in each time frame $d = 1, ..., 67$ were divided into narrow band sequences of 1 Hz band each. The bands overlap by 2^{-5} Hz resulting in 929 bands numbered from 0 to 928. The relation between the band number b and the offset frequency $f_{\rm off}$ is thus given by

$$f_{\rm off}\,[\mathrm{Hz}] = 100 + \left(1 - 2^{-5}\right)b. \tag{1}$$

Consequently, we have 62 243 narrow band data segments. From this set we selected good data using the following conditions. Let N_0 be the number of zeros in a given data segment (a data value at a given time is set exactly to 0 whenever at that time there are no science data). Let $[f_{\rm off}, f_{\rm off} + B]$ be the band of a given data segment. Let $S_{\rm min}$ and $S_{\rm max}$ be the minimum and the maximum of the amplitude spectral density in the interval $[f_{\rm off} + 0.05B, f_{\rm off} + B - 0.05B]$. Spectral density was estimated by dividing the data of a given segment into short stretches and averaging spectra of all the short stretches. We consider the data segment as good data and use it in this analysis, if the following two criteria, selected as a rule of thumb, are met:

1. $N_0/N < 1/4$,
2. $S_{\rm max}/S_{\rm min} \leqslant 1.1$.

20 419 data segments met the above two criteria. Figure 2 shows a time–frequency distribution of the good data segments. The good data appeared in 50 out of 67 two-day time frames and in 785 out of 929 bands. The distribution of good data segments in time frames and in bands is given in figure 3. In figure 4 we plot a snapshot spectral density of VSR1 data presented in figure 1 and an estimate of the spectral density of the data that were used in the analysis. We estimate the spectral density in each band by a harmonic mean of the spectral densities of each of the two-day time segments chosen for the analysis in the band. As the data spectrum in each band is approximately white, we estimate the spectral density in each

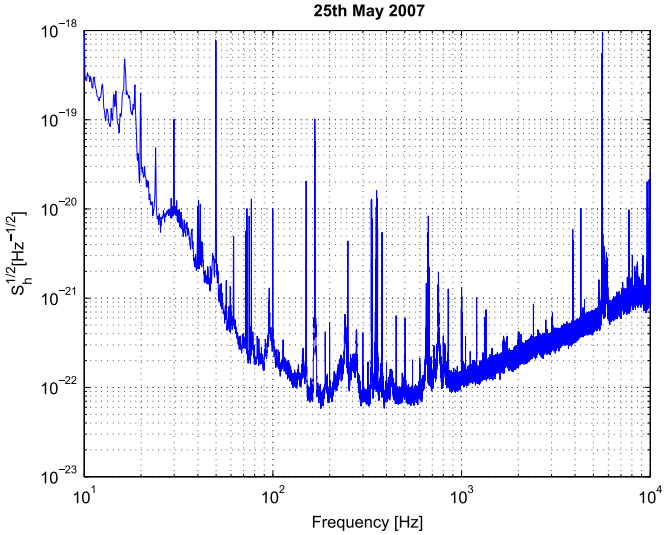

Figure 1. Strain amplitude spectral density $\sqrt{S_h}$ of Virgo data taken on 25 May 2007 during the VSR1 run.

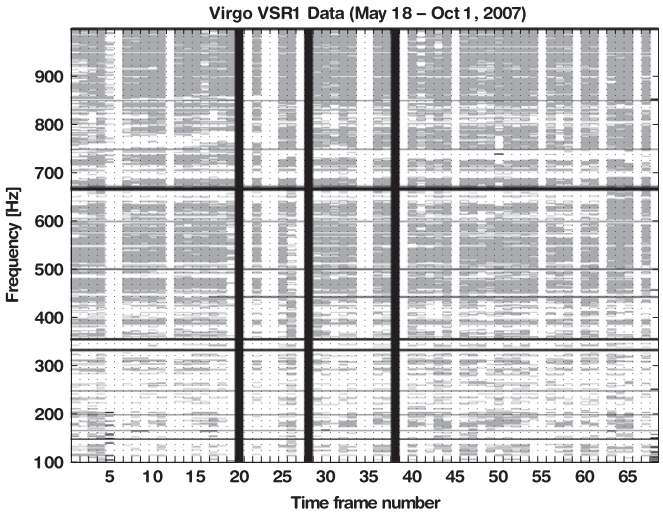

Figure 2. A map of the VSR1 data. Grey—good data selected for the analysis, white—data not analyzed because of large number of missing data or a strong variation of the spectrum, black—bad data where number of missing data is greater than 50% or there are strong lines from mirror wires, electronics, etc.

time segment by $2\sigma^2\Delta t$, where σ^2 is the variance of the data in a segment and Δt is the 1/2 s sampling time. We plot the band from 100 Hz to 1 kHz, which we have chosen for this search.

4. The response of the detector

The dimensionless noise-free response h of a gravitational-wave detector to a weak plane gravitational wave in the *long wavelength approximation*, i.e., when the characteristic size of

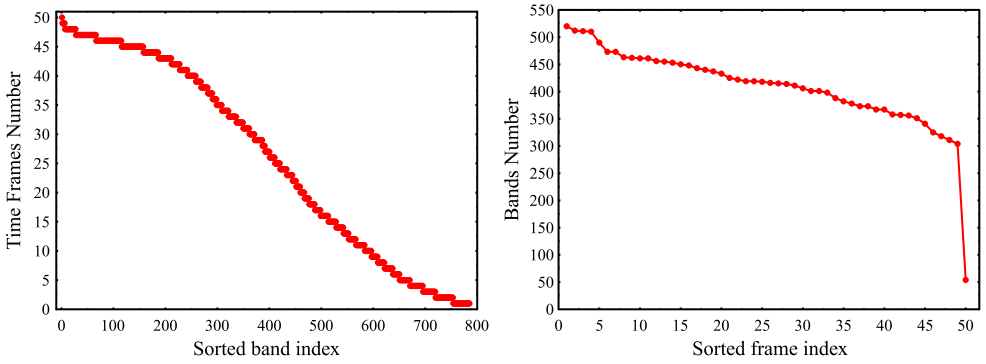

Figure 3. Number of good data segments. Left panel—distribution of data segments in frequency bands. The number of data segments chosen for the analysis in a given frequency band varies from 1 to 50. Right panel—distribution of data segments time frames. The number of data segments in a given time frame varies from 54 to 520. The smallest, outlying number of bands of 54 is in the 5th time frame. In the remaining frames the number of good bands is greater than 300.

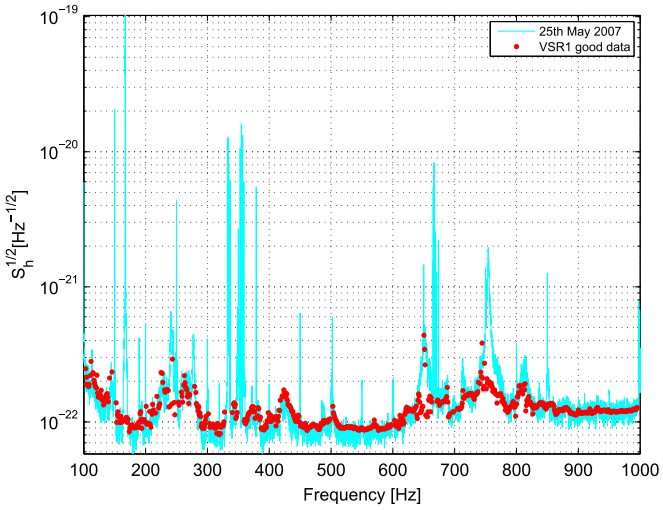

Figure 4. A snapshot of strain amplitude spectral density $\sqrt{S_h}$ of the VSR1 data (solid curve) in comparison with the spectral density estimated from the data used in the analysis (dots). The spectrum in each band is obtained from a harmonic mean of the spectral densities of the data in each segment chosen for the analysis in the band.

the detector is much smaller than the reduced wavelength $\lambda/(2\pi)$ of the wave, can be written as the linear combination of the two independent wave polarizations h_+ and $h_\times$,

$$h(t) = F_+(t)h_+(t) + F_\times(t)h_\times(t), \tag{2}$$

where F_+ and $F_\times$ are the detector's beam-pattern functions,

$$F_+(t) = a(t)\cos 2\psi + b(t)\sin 2\psi, \tag{3}$$

$$F_{\times}(t) = b(t)\cos 2\psi - a(t)\sin 2\psi. \tag{4}$$

The beam-patterns F_+ and $F_\times$ are linear combinations of $\sin 2\psi$ and $\cos 2\psi$, where ψ is the polarization angle of the wave. The functions $a(t)$ and $b(t)$ are the amplitude modulation functions, that depend on the location and orientation of the detector on the Earth and on the position of the gravitational-wave source in the sky, described in the equatorial coordinate system by the right ascension α and the declination δ angles. They are periodic functions of time with the period of one and two sidereal days. The analytic form of the functions $a(t)$ and $b(t)$ for the case of interferometric detectors is given by equations (12) and (13) of [17]. For a rotating non-axisymmetric neutron star, the wave polarization functions are of the form

$$h_+(t) = h_{0+}\cos\Big(\phi(t) + \phi_0\Big), \qquad h_\times(t) = h_{0\times}\sin\Big(\phi(t) + \phi_0\Big), \tag{5}$$

where h_{0+} and $h_{0\times}$ are constant amplitudes of the two polarizations and $\phi(t) + \phi_0$ is the phase of the wave, ϕ_0 being the initial phase of the waveform. The amplitudes h_{0+} and $h_{0\times}$ depend on the physical mechanism responsible for the gravitational radiation, e.g., if a neutron star is a triaxial ellipsoid rotating around a principal axis with frequency f, then these amplitudes are

$$h_{0+} = \frac{1}{2}h_0\Big(1 + \cos^2\iota\Big), \qquad h_{0\times} = h_0\cos\iota, \tag{6}$$

where ι is the angle between the star's angular momentum vector and the direction from the star to the Earth, and the amplitude h_0 is given by

$$h_0 = \frac{16\pi^2 G}{c^4}\frac{\epsilon I f^2}{r}. \tag{7}$$

Here I is the star's moment of inertia with respect to the rotation axis, r is the distance to the star and ϵ is the star's ellipticity defined by $\epsilon = |I_1 - I_2|/I$, where I_1 and I_2 are moments of inertia with respect to the principal axes orthogonal to the rotation axis. We assume that the gravitational waveform given by equations (2)–(5) is almost monochromatic around some angular frequency ω_0, which we define as instantaneous angular frequency evaluated at the solar system barycenter (SSB) at $t = 0$, and we assume that the frequency evolution is accurately described by one spindown parameter ω_1. Then the phase $\phi(t)$ is given by

$$\phi(t) = \omega_0 t + \omega_1 t^2 + \frac{\mathbf{n}\cdot\mathbf{r}_d(t)}{c}\big(\omega_0 + 2\omega_1 t\big), \tag{8}$$

where, neglecting the relativistic effects, $\mathbf{r}_d(t)$ is the vector that joins the SSB with the detector, and $\mathbf{n}$ is the unit vector pointing from SSB to the source. In equatorial coordinates (δ, α) we have $\mathbf{n} = (\cos\delta\cos\alpha, \cos\delta\sin\alpha, \sin\delta)$.

5. The $\mathcal{F}$-statistic

A method to search for gravitational wave signals from a rotating neutron star in detector data $x(t)$, $t = 1, \ldots, N$ uses the $\mathcal{F}$-statistic, described in [17]. The $\mathcal{F}$-statistic is obtained by maximizing the likelihood ratio function with respect to the four unknown parameters—h_0, ϕ_0, ι, and ψ. This leaves a function of only the remaining four parameters—ω_0, ω_1, δ, and α. Thus the dimension of the parameter space that we need to search decreases from 8 to 4. In this analysis we shall use an observation time $T_{\rm obs}$ equal to the integer multiple of sidereal days. Since the bandwidth of the signal over our coherent observation time of two days is very small, we can assume that over this band the spectral density of the noise is white

(constant). Under these assumptions the $\mathcal{F}$-statistic is given by [25, 26]

$$\mathcal{F} \approx \frac{2}{\sigma^2}\left(\frac{|F_a|^2}{\langle a^2\rangle} + \frac{|F_b|^2}{\langle b^2\rangle}\right), \tag{9}$$

where σ^2 is the variance of the data, and

$$\begin{aligned} F_a &:= \sum_{t=1}^{N} x(t)a(t)\exp\left[-\mathrm{i}\phi(t)\right], \\ F_b &:= \sum_{t=1}^{N} x(t)b(t)\exp\left[-\mathrm{i}\phi(t)\right]. \end{aligned} \tag{10}$$

$$\langle a^2\rangle = \sum_{t=1}^{N} a(t)^2, \quad \langle b^2\rangle = \sum_{t=1}^{N} b(t)^2. \tag{11}$$

6. Description of the search

The search consists of two parts; the first part is a coherent search of two-day data segments, where we search a 4-parameter space defined by angular frequency ω_0, angular frequency derivative ω_1, declination δ and right ascension α. The search is performed on a 4-dimensional grid in the parameter space described in section 6.2. We set a fixed threshold of **20** for the $\mathcal{F}$-statistic for each data segment. This corresponds to a threshold of **6** for the signal-to-noise ratio. All the threshold crossings are recorded together with the corresponding four parameters of the grid point and the signal-to-noise ratio ρ. The signal-to-noise is calculated from the value of the $\mathcal{F}$-statistic at the threshold crossing as

$$\rho = \sqrt{2(\mathcal{F} - 2)}\,. \tag{12}$$

In this way, for each narrow band segment we obtain a set of candidates. The candidates are then subject to the vetoing procedure described in section 7. The second part of the search is the post-processing stage involving search for coincidences among the candidates. The coincidence procedure is described in section 8.

6.1. Choice of the parameter space

We have searched the frequency band from 100 Hz to 1 kHz over the entire sky. We have followed [12] to constrain the maximum value of the parameter ω_1 for a given frequency ω_0 by $|\omega_1| \leqslant \omega_0/(2\tau_{\min})$, where $\tau_{\min}$ is the minimum spindown age[128]. We have chosen $\tau_{\min} = 1000$ yr for the whole frequency band searched. Also, in this search we have considered only negative values for the parameter ω_1, thus assuming that the rotating neutron star is spinning down. This gives the frequency-dependent range of the spindown parameter f_1 where $f_1 = \omega_1/(2\pi)$:

$$\left|f_1\right| \leqslant 1.6 \times 10^{-9} \frac{f}{100\ \mathrm{Hz}} \frac{1000\ \mathrm{yr}}{\tau_{\min}} \left[\mathrm{Hz\ s^{-1}}\right]. \tag{13}$$

[128] The factor of two in this formula appears here because the spindown parameter $\dot{f}$ used in [12] is twice the spindown parameter used in this work.

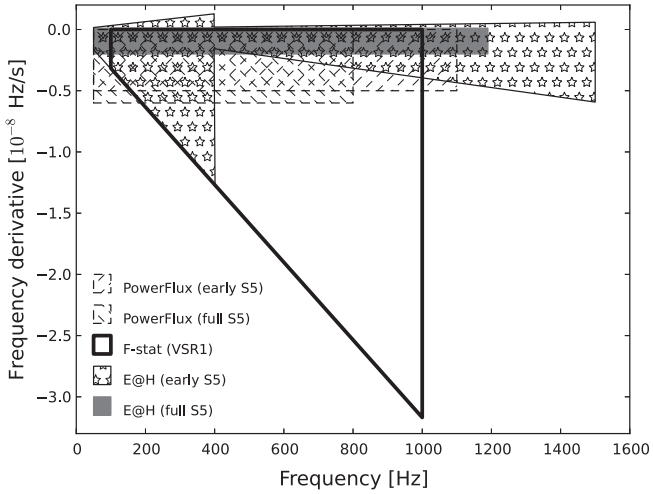

Figure 5. Comparison of the parameter space in $f-\dot{f}$ plane searched in VSR1 analysis presented in this paper (area enclosed by a thick black line) and recently published PowerFlux and E@H searches of the LIGO S5 data.

We have considered only one frequency derivative. Estimates taking into account parameter correlations (see [12] figure 6 and equations (6.2)–(6.6)) show that even for the minimum spindown age of 40 yr and for two days coherent observation time that we consider here, it is sufficient to include just one spindown parameter.

In figure 5 we have compared the parameter space searched in this analysis in the $f-\dot{f}$ plane with that of other recently published all-sky searches: Einstein@Home early S5 search [20], Einstein@Home full S5 [21], PowerFlux early S5 [27], PowerFlux full S5 [16].

6.2. Efficient calculation of the $\mathcal{F}$-statistic on the grid in the parameter space

Calculation of the $\mathcal{F}$-statistic (equation (9)) involves two sums given by equation (10). By introducing a new time variable called the barycentric time t_b ([17, 26, 28])

$$t_b := t + \frac{\mathbf{n}\cdot\mathbf{r}_d(t)}{c}. \tag{14}$$

we can write these sums as discrete Fourier transforms in the following way

$$\begin{aligned} F_a &= \sum_{t_b=1}^{N} x\big(t(t_b)\big)a\big(t(t_b)\big)\exp\Big[-\mathrm{i}\phi_s\big(t(t_b)\big)\Big]\exp\big[-\mathrm{i}\omega_0 t_b\big], \\ F_b &= \sum_{t_b=1}^{N} x\big(t(t_b)\big)b\big(t(t_b)\big)\exp\Big[-\mathrm{i}\phi_s\big(t(t_b)\big)\Big]\exp\big[-\mathrm{i}\omega_0 t_b\big], \end{aligned} \tag{15}$$

where

$$\phi_s(t) = \omega_1 t^2 + 2\frac{\mathbf{n}\cdot\mathbf{r}_d(t)}{c}\omega_1 t. \tag{16}$$

The values of $x(t(t_b))a(t(t_b))\exp[-\mathrm{i}\phi_s(t(t_b))]$ in equation (15) above that are evaluated at barycentric time t_b are obtained from the values in equation (10) evaluated at time t by an

interpolation procedure described in section VIA of [26]. The procedure consists of upsampling using the Fourier transform, followed by a spline interpolation.

Written in this form, the two sums can be evaluated using the fast Fourier transform (FFT) algorithm thus speeding up their computation dramatically. The time transformation described by equation (14) is called *resampling*. In addition to the use of the FFT algorithm we apply an interpolation of the FFT using the interbinning procedure (see [26], section VB). This results in the $\mathcal{F}$-statistic sampled twice as fine with respect to the standard FFT. This procedure is much faster than the interpolation of the FFT obtained by padding the data with zeros and calculating a FFT that is twice as long. With the approximations described above for each value of the parameters ω_1, δ and α, we calculate the $\mathcal{F}$-statistic efficiently for all the frequency bins in the data segment of bandwidth 1 Hz.

In order to search the four-dimensional parameter space, we need to construct a four-dimensional grid. To minimize the computational cost we construct a grid that has the smallest number of points for a certain assumed *minimal match MM* [29]. This problem is equivalent to the *covering problem* [30, 31] and it has the optimal solution in four dimensions in the case of a *lattice*, i.e., a uniformly spaced grid. In order that our parameter space is a lattice, the signals' reduced Fisher matrix must have components that are independent of the values of the parameters. This is not the case for the signal given by equations (2)–(8); it can be realized however for an approximate signal called the *linear model* described in section IIIB of [26]. The linear model consists of neglecting amplitude modulation of the signal and discarding the component of the vector $\mathbf{r}_d(t)$ joining the detector and the solar system barycenter that is perpendicular to the ecliptic. This approximation is justified because the amplitude modulation is very slow compared to the phase modulation and the discarded component in the phase is small compared to the others. As a result the linear model signal $h_{\mathrm{lin}}(t)$ has a constant amplitude A_0, and one can find parameters such that the phases are linear functions of them. We explicitly have (see section IIIB of [26] for details):

$$h_{\mathrm{lin}}(t) = A_0 \cos\Big[\phi_{\mathrm{lin}}(t) + \phi_0\Big], \tag{17}$$

where

$$\phi_{\mathrm{lin}}(t) = \omega_0 t + \omega_1 t^2 + \alpha_1\mu_1(t) + \alpha_2\mu_2(t). \tag{18}$$

The parameters α_1 and α_2 are defined by

$$\begin{aligned} \alpha_1 &:= \omega_0(\sin\alpha\cos\delta\cos\varepsilon + \sin\delta\sin\varepsilon), \\ \alpha_2 &:= \omega_0\cos\alpha\cos\delta, \end{aligned} \tag{19}$$

where ε is the obliquity of the ecliptic, and $\mu_1(t)$ and $\mu_2(t)$ are known functions of the detector ephemeris.

In order that the grid is compatible with application of the FFT, its points should be constrained to coincide with Fourier frequencies at which the FFT is calculated. Moreover, we observed that a numerically accurate implementation of the interpolation to the barycentric time (see equation (14)) is so computationally demanding that it may offset the advantage of the FFT. Therefore we introduced another constraint in the grid such that the resampling is needed only once per sky position for all the spindown values. Construction of the constrained grid is described in detail in section IV of [26]. In this search we have chosen the value of the minimal match $MM = \sqrt{3}/2$. The workflow of the coherent part of the search procedure is presented in figure 6.

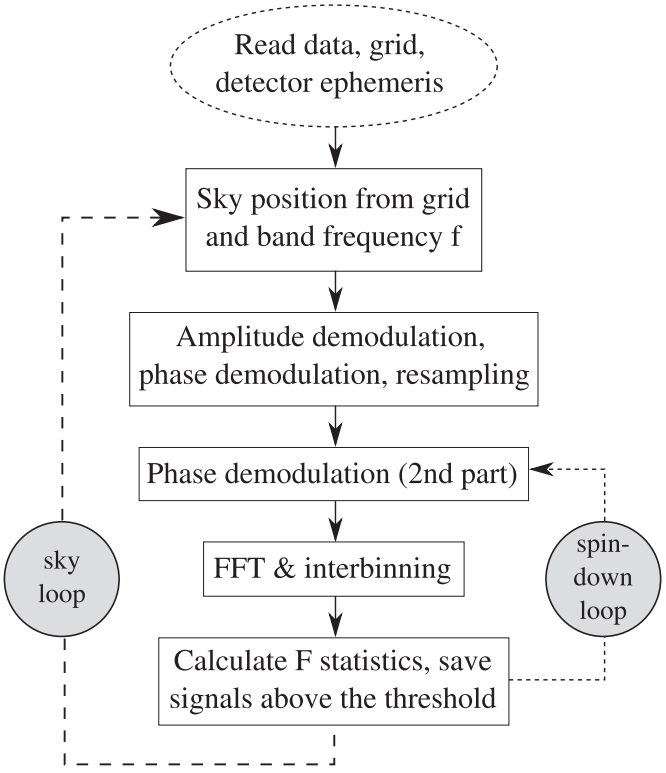

Figure 6. Workflow of the $\mathcal{F}$-statistic search pipeline.

7. Vetoing procedure

We apply three vetoing criteria to the candidates obtained in the coherent part of the search—line width veto, stationary line veto and polar caps veto. Data from the detector always contain some periodic interferences (lines) that are detector artifacts. An important part of our vetoing procedure was to identify the lines in the data. We have therefore performed a Fourier search with frequency resolution of $1/(2\ \text{days}) \simeq 5.8 \times 10^{-6}$ Hz for periodic signals of each of the two-day data segments. We compared the frequencies of the significant periodic signals identified by our analysis with the line frequencies obtained by the Virgo LineMonitor and we found that all the lines from the LineMonitor were detected by our Fourier search.

7.1. Line width veto

We veto all the candidates with frequency f around every known line frequency f_l according to the following criterion

$$\left|f - f_l\right| < \Delta f_{\max} \tag{20}$$

where the width $\Delta f_{\max}$ is estimated as

$$\Delta f_{\max} = f_l |v|_{\max}/c + 2\left|f_1\right|_{\max}\left(T_{\text{obs}} + T_{\text{obs}}|v|_{\max}/c + |r|_{\max}/c\right), \tag{21}$$

where $v_{\max}$ is the maximum value of the velocity of the detector with respect to the SSB during the observation time, $r_{\max}$ is the maximum distance to the SSB during the coherent observation time $T_{\rm obs}$ and $|f_1|_{\max}$ is the maximum of the absolute value of the frequency derivative. Equation (21) determines the maximum smearing of the frequency on each side of the line due to frequency modulation induced by the filters applied in the $\mathcal{F}$-statistic.

7.2. Stationary line veto

Let us consider the instantaneous frequency $f_{\rm inst}$ of the signal, i.e., the time derivative of the phase:

$$f_{\rm inst} := \frac{1}{2\pi}\frac{{\rm d}\phi(t)}{{\rm d}t} = f_0 + 2f_1 t + \frac{\mathbf{n}\cdot\mathbf{v}_d(t)}{c}\left(f_0 + 2f_1 t\right) + 2\frac{\mathbf{n}\cdot\mathbf{r}_d(t)}{c}f_1, \qquad (22)$$

where $\mathbf{v}_d(t) = {\rm d}\mathbf{r}_d(t)/{\rm d}t$. The frequency derivative of the instantaneous frequency is given by

$$\frac{{\rm d}f_{\rm inst}(t)}{{\rm d}t} = 2f_1 + \frac{\mathbf{n}\cdot\mathbf{a}_d(t)}{c}\left(f_0 + 2f_1 t\right) + 4\frac{\mathbf{n}\cdot\mathbf{v}_d(t)}{c}f_1, \qquad (23)$$

where $\mathbf{a}_d(t) = {\rm d}\mathbf{v}_d(t)/{\rm d}t$. Equation (23) is the rate of change of detector response frequency for a source whose SSB frequency and spindown are f_0 and f_1. An instrumental line has a constant detector frequency and mimics a source for which the r.h.s of equation (23) vanishes. In practice, we veto candidates with

$$\left|2f_1 + \frac{\mathbf{n}\cdot\mathbf{a}_d(t)}{c}f_0 + 2\frac{\mathbf{n}\cdot d^2\left(\mathbf{r}_d(t)t\right)/{\rm d}t^2}{c}f_1\right| < \epsilon_{SL} \qquad (24)$$

for some $\epsilon_{SL} > 0$. In the search we choose $\epsilon_{SL} = 1/T_{\rm obs}^2$, where $T_{\rm obs}$ is the observation time. The above stationary line veto was introduced in [13] and refined in [32]; it was used in the first two E@H searches [19, 20].

7.3. Polar caps veto

We observe that many of the detected lines cluster around the poles where declination δ is close to $\pm\pi/2$. An interference originating from a detector will correlate well with our templates if the frequency modulation in equation (22) is minimized. Assuming that $f_1 = 0$ and that the diurnal motion of the Earth averages to 0 over two days observation time, this happens when the quantity $|\mathbf{n}\cdot\mathbf{v}_d(t)|$ is minimized. We find that this quantity is close to minimum independently of the value of α when $\delta = \pm\pi/2$. Thus we veto candidates that are too close to the poles; we discard all candidates with the declination angle δ within three grid cells from the poles.

8. Coincidences

In order to find coincidences among the candidates, we applied a method similar to the one used in the first two E@H searches [19, 20]. For each band we have searched for coincidences among candidates in different time frames. We are able to search for coincidences only in those bands where there were two or more time frames with data selected for the analysis. If we search for a real gravitational wave signal, we must take into account frequency evolution due to spindown of the rotating neutron star. Thus the first step in the coincidence analysis was to transform all frequencies $\omega_0(t_l)$ of the candidates to a common fiducial reference time t_f. We have chosen the fiducial time to be the time of the first sample of the latest time frame

that we analyzed, i.e., the 67th time frame. We have

$$\omega\left(t_f\right) = \omega_0(t_l) + 2\,\omega_1(t_l)\left[67\,T_{\rm obs} - t_l\right], \tag{25}$$

where t_l is the time of the first sample of the lth time frame. The next step was to divide the parameter space into cells. This construction of the coincidence cell was different from that in the E@H analysis. To construct the cells in the parameter space we have used the reduced Fisher matrix $\tilde{\Gamma}$ for the linear signal model defined by equations (17) and (18). The reduced Fisher matrix is the projected Fisher matrix on the 4-dimensional space spanned by parameters $\kappa = (\omega_0, \omega_1, \alpha_1, \alpha_2)$. We define the cell in the parameter space by the condition:

$$\sum_{k,l} \tilde{\Gamma}_{kl}\kappa_k\kappa_l \leqslant 2. \tag{26}$$

Because the ephemeris of the detector is different in each of the time frames, the reduced Fisher matrix is different in each time frame. To have a common coincidence grid we have chosen the grid defined by the latest frame, i.e., the frame no. 67 as the coincidence grid. After the transformation of the candidate frequencies to a reference time and construction of the coincidence grid, the coincidence algorithm for each of the bands proceeded in the following steps:

1. Transform angles α and δ to α_1 and α_2 coordinates (see equation (19))
2. Transform candidate parameters to x_l coordinates defined by

$$x_l = \sum_{k=1}^{4} \kappa_k\, V_{kl}\,\sqrt{e_l}, \tag{27}$$

   where V_{kl}, $k = 1,..,4$ are eigenvectors of the matrix $\tilde{\Gamma}$, and e_l are its eigenvalues. In these coordinates the Fisher matrix is proportional to the unit matrix.
3. Coordinates x_l are rounded to the nearest integer. In this way we sort candidates efficiently into adjacent four-dimensional hypercubes. If there are more than one candidates from a given data segment in a hypercube we select the candidate that has the highest SNR. We do sorting for each time frame in the band. If there is more than one candidate in a given hypercube we register a coincidence.
4. We shift cubes by 1/2 of their size in all possible 2^4 directions, and for each shift we search for coincidences.

This last step of the algorithm takes into account cases for which the candidate events are located on opposite sides of cell borders, edges and corners and consequently coincidences that could not be found just by packing candidates into adjacent cells.

The most significant coincidence in each band is the one which has the highest multiplicity. For each most significant coincidence we have calculated the false alarm probability i.e., the probability that such a coincidence can occur purely by chance. The false alarm probability is calculated using the formula explained in the appendix and given by equation (A.6). This general formula applies to a variable number of candidates in various time slots and also takes into account the 2^4 shifts of the cells in the parameter space.

9. The search

In this analysis we have searched coherently 20 419 two-day time segments of data narrowbanded to 1 Hz. The analysis took approximately 15 months and involved several big computing clusters. During the analysis 1000–3000 computing cores were used continuously.

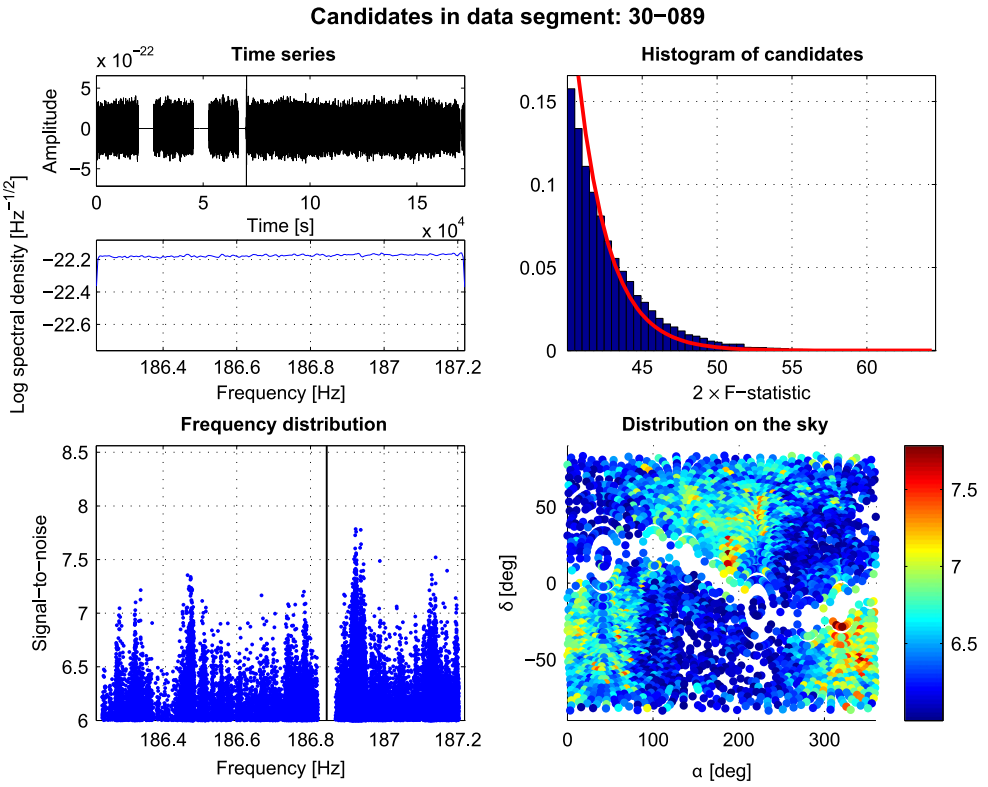

Figure 7. Distribution of candidates after vetoing obtained in the coherent $\mathcal{F}$-statistic search of two-day data segment 30−089 i.e., a segment with the time frame number $d = 30$ and the band number $b = 89$. The left top panel shows data and their spectrum. The right top panel shows the distribution of $2\mathcal{F}$ values of the candidates in comparison to the χ^2 distribution with four degrees of freedom. The bottom left panel shows the distribution of signal-to-noise ratios ρ (see equation (12)) of the candidates as a function of the frequency. The vertical black line is the periodic interference identified in the data. The candidates in the band around the line are vetoed (see equation (21)). The right bottom panel shows the distribution of the candidates on the sky in equatorial coordinates α and δ.

In the coherent part of the search described in section 6 we have used 9.10×10^{16} templates, which is the number of $\mathcal{F}$-statistic values computed. This resulted in 20 419 candidate files containing 4.21×10^{10} candidates. The candidates were subject to vetoing using three veto criteria: line veto, polar caps veto and stationary line veto described in section 7. As a result of vetoing around 24% of the candidates were discarded leaving 3.19×10^{10} candidates. Nearly all candidates were vetoed by the line veto, whereas 0.20% were vetoed by the stationary line criterion and only 3.2×10^{-2}% by the polar caps veto. In figure 7 we present an example of the candidate distribution obtained from the coherent search of one narrow band data segment and after the vetoing procedure. In the search the celestial sphere is divided by the ecliptic plane into two hemispheres. Each hemisphere is mapped onto the disc defined by $(\alpha_1^2 + \alpha_2^2)/\omega_0^2 \leqslant 1$, where the coordinates α_1 and α_2 are defined by equation (19) and ω_0 is the angular frequency. The edge of the disc, determined by condition $(\alpha_1^2 + \alpha_2^2)/\omega_0^2 = 1$, is precisely the ecliptic. At this edge the grid of templates degenerates. This degeneracy

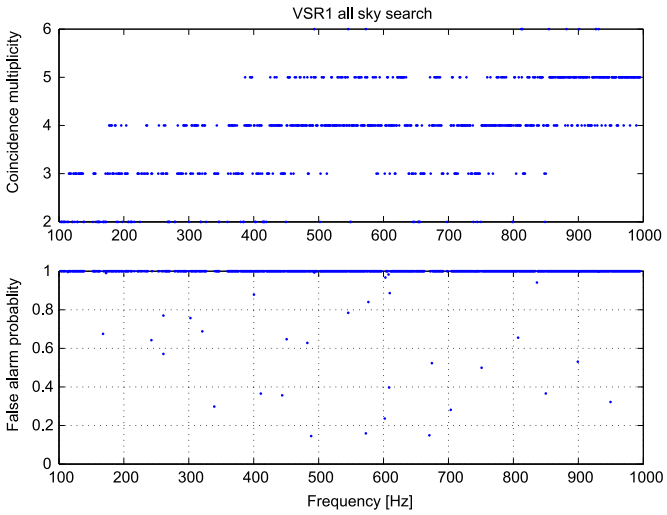

Figure 8. Coincidences among the candidates. Top panel: maximum multiplicity of coincidence as function of frequency. Bottom panel: corresponding coincidence false alarm probability.

manifests itself as a gap in the distribution of candidates on the sky (bottom right panel in figure 7), which follows exactly the ecliptic in the equatorial coordinates δ and α.

In the next step we have searched for the significant coincidences among the candidates. We have searched for coincidences in all the frequency bands where there were two or more data segments analyzed. In figure 8 we have plotted the highest coincidence multiplicity for each of the bands. The highest multiplicity was 6, and it occurred in 10 bands. The multiplicity tends to grow with the frequency, because the size of the parameter space grows as f^3. For each band we have calculated the false alarm probability corresponding to the most significant coincidence using equation (A.6). The most significant coincidence occurred in band no. 401, corresponding to the frequency range of $\sim$[488.4, 489.4] Hz. It was a coincidence of multiplicity = 5, and its false alarm probability was 14.5%. Note that a coincidence with the highest multiplicity is not the most significant. This is because the significance depends on the number of time frames with candidates in a given band and also on the number of candidates in the time frames. By adopting a criterion used by E@H searches that the background coincidences correspond to false alarm probability of 0.1% or greater, we conclude that we have found no significant coincidence and thus no viable gravitational wave candidate. Considering the significance of the coincidences, we could adopt even a 10% false alarm probability as a background. Consequently, we proceed to the final stage of our analysis —estimation of sensitivity of the search.

10. Sensitivity of the search

The sensitivity of the search is taken to be the amplitude h_0 of the gravitational wave signal that can be confidently detected. To estimate the sensitivity we use a procedure developed in [19]. We determine the sensitivity of the search in each of the 785 frequency bands that we have searched. To determine the sensitivity, we perform Monte-Carlo simulations in which, for a given amplitude h_0, we randomly select the other seven parameters of the signal:

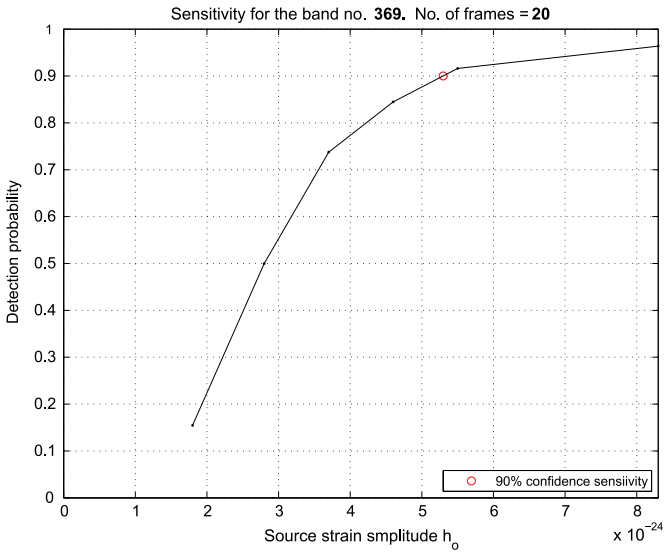

Figure 9. Estimation of sensitivity in the band no. 369. In this band there are 20 time frames. Thus the signal is detected if it is coincident in more than 14 frames. The black dots are amplitudes of the injected signals and the corresponding detection probabilities estimated from the injections. The red circle is the interpolated amplitude corresponding to 90% detection probability. This is the 90% confidence sensitivity for this band.

ω_0, ω_1, α, δ, ϕ_0, ι and ψ. We choose frequency and spindown parameters uniformly over their range, and source positions uniformly over the sky. We choose angles ϕ_0 and ψ uniformly over the interval $[0, 2\pi]$ and we choose $\cos\iota$ uniformly over the interval $[-1, 1]$. For each band we add the signal to all the data segments chosen for the analysis in that band. Then we process the data through our pipeline. First, we perform a coherent $\mathcal{F}$-statistic search of each of the data segments where the signal was added, and store all the candidates above our $\mathcal{F}$-statistic threshold of 20. In this coherent analysis, to make the computation manageable, we search over only parameter space consisting of ± 2 grid points around the nearest grid point where the signal was added. Then we apply our vetoing procedure to the candidates obtained as explained in section 7. Finally, we perform coincidence analysis of the candidates that survive vetoing, which is described in section 8. We define a detectable signal if it is coincident in more than 70% of the time frames in a given band. This condition is similar to the condition used in the two E@H searches, where a coincidence method was used [19, 20]. For bands with only one frame available, the coherent search over one 2-day data segment was performed. In this case the injected signal is declared detected if its signal-to-noise ratio obtained in the coherent search is larger than the signal-to-noise ratio of the loudest signal in that data segment without an injection. For each band we inject signals with five different amplitude values, and perform 100 randomized injections for each amplitude. For each amplitude we calculate how many signals were detected, and by interpolation we determine the amplitude corresponding to 90% of signals detected. This amplitude was defined as the 90% confidence sensitivity. Sometimes even for the highest amplitude we have not reached the 90% detection probability. In this case we performed injections for higher amplitudes until the desired level of detectability was achieved. In figure 9, as an example, we present an estimation of the sensitivity in the band $b = 369$ corresponding to the frequency range of

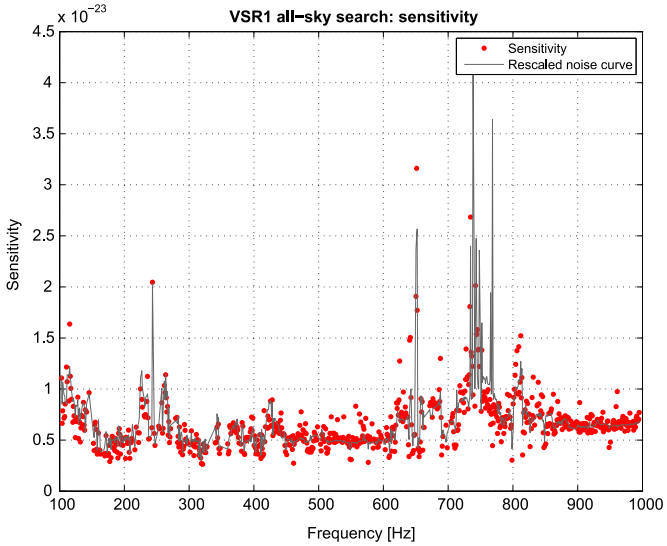

Figure 10. The 90% confidence sensitivity of the all-sky search of Virgo VSR1 data in the band from 100 Hz to 1 kHz. The dots show the source strain amplitude h_0 for which 90% of sources are confidently detected by this pipeline. The thin line is the rescaled instrumental noise curve, see equation (28).

$\sim$[457.47, 458.44] Hz. The errors in the sensitivity estimates originate from calibration errors in the amplitude and errors due to a finite number of Monte-Carlo injections. We use 100 injections; hence from a binomial statistic, one σ is equivalent to 3% fluctuation. Thus the estimated amplitude sensitivity corresponds to confidence in the range from 87% to 93%. To estimate how this uncertainty in confidence translates into uncertainty in the amplitude we have performed an additional set of injections for a range of amplitudes close to the estimated sensitivity and from the slope of the confidence versus amplitude we determined the uncertainty in the amplitude. To increase the accuracy of the error estimate, we have performed 1000 injections for each amplitude. The uncertainty in the amplitude was not more than 5%. The calibration errors in VSR1 data are 6% (see section 2). Adding these two types of errors in quadrature results in the total error in sensitivity estimate to be around 7%. The sensitivity of this search obtained through Monte-Carlo simulations for the whole band searched is presented in figure 10. We see from figure 10 that the sensitivity essentially reflects the instrumental noise curve given in figure 4. We have made a fit of the sensitivity $h_0^{90\%}$ to the one-sided spectral density $S_h(f)$ of detector noise described by the following relation:

$$h_0^{90\%} = R_{\mathcal{D}} \sqrt{\frac{S_h(f)}{48 \text{ hours}}}. \tag{28}$$

We find that the prefactor $R_{\mathcal{D}}$ is in the range from 15.6 to 22.4 and it depends on the frequency band and the number of data segments in the band.

11. Conclusions

The sensitivity of this search was 50% to 2 times better, depending on the bandwidth, than that of the LIGO S4 search [19] and comparable to the sensitivities obtained in the early LIGO S5 data [20], but 2 to 5 times worse than the upper limits in the E@H full LIGO S5 data search [21]. This was due to the lower noise and longer observation time for the LIGO S5 data w.r.t the Virgo VSR1 data. However, for the first time in an all-sky search we have estimated the sensitivity in the frequency band from 400 Hz to 1 kHz and the frequency spindown range from $-7.2(f_0/400\,\mathrm{Hz}) \times 10^{-9}\,\mathrm{Hz\,s^{-1}}$ to $-6.0 \times 10^{-9}\ \mathrm{Hz\,s^{-1}}$, which is a previously unexplored region in the parameter space.

The next step is to test the search method described in this paper in the Mock Data Challenge (MDC) designed by the LIGO and Virgo projects to validate and compare pipelines that are proposed to be used in the analysis of the forthcoming data from the advanced detectors. It is also planned to further test the pipeline presented here with other data sets collected by the LIGO and Virgo detectors.

Acknowledgments

The authors gratefully acknowledge the support of the United States National Science Foundation for the construction and operation of the LIGO Laboratory, the Science and Technology Facilities Council of the United Kingdom, the Max-Planck-Society and the State of Niedersachsen/Germany for support of the construction and operation of the GEO600 detector, and the Italian Istituto Nazionale di Fisica Nucleare and the French Centre National de la Recherche Scientifique for the construction and operation of the Virgo detector. The authors also gratefully acknowledge the support of the research by these agencies and by the Australian Research Council, the International Science Linkages program of the Commonwealth of Australia, the Council of Scientific and Industrial Research of India, the Istituto Nazionale di Fisica Nucleare of Italy, the Spanish Ministerio de Economía y Competitividad, the Conselleria d'Economia Hisenda i Innovació of the Govern de les Illes Balears, the Foundation for Fundamental Research on Matter supported by the Netherlands Organisation for Scientific Research, the Polish Ministry of Science and Higher Education, the FOCUS Programme of Foundation for Polish Science, the PL-Grid Infrastructure, the Royal Society, the Scottish Funding Council, the Scottish Universities Physics Alliance, The National Aeronautics and Space Administration, the Carnegie Trust, the Leverhulme Trust, the David and Lucile Packard Foundation, the Research Corporation, and the Alfred P Sloan Foundation. This document has been assigned LIGO Laboratory document number LIGO-P1300133.

Appendix. False alarm coincidence probability

Let us assume that for a given frequency band we analyze L non-overlapping time segments. Suppose that the search of the lth segment produces N_l candidates. Let us assume that the size of the parameter space for each time segment is the same, and it can be divided into the number N_{cell} of independent cells. We would like to test the null hypothesis that coincidences among candidates from L segments are accidental. The probability for a candidate event to fall into any given coincidence cell is equal to $1/N_{\mathrm{cell}}$. Thus probability ϵ_1 that a given coincidence cell is populated with one or more candidate events is given by

$$\epsilon_l = 1 - \left(1 - \frac{1}{N_{\rm cell}}\right)^{N_l}. \tag{A.1}$$

We may also consider independent candidates only, i.e., such that there is no more than one candidate within one cell. If we obtain more than one candidate within a given cell we choose the one which has the highest signal-to-noise ratio. In this case

$$\epsilon_l = \frac{N_l}{N_{\rm cell}}. \tag{A.2}$$

The probability $p_F\,(N_{\rm cell})$ that any given coincidence cell out of the total of $N_{\rm cell}$ cells contains candidate events from $C_{\rm max}$ or more distinct data segments is given by a generalized binomial distribution

$$p_F\left(N_{\rm cell}\right) = \sum_{n=C_{\rm max}}^{L} \frac{1}{n!(L-n)!} \sum_{\sigma\in\Pi(L)} \epsilon_{\sigma(1)}\ldots\epsilon_{\sigma(n)}\left(1-\epsilon_{\sigma(n+1)}\right)\ldots\left(1-\epsilon_{\sigma(L)}\right), \tag{A.3}$$

where $\sum_{\sigma\in\Pi(L)}$ is the sum over all the permutations of the L data sequences. Finally the probability P_F that there is $C_{\rm max}$ or more coincidences in one or more of the $N_{\rm cell}$ cells is

$$P_F = 1 - \left(1 - p_F\left(N_{\rm cell}\right)\right)^{N_{\rm cell}}. \tag{A.4}$$

The above formula for the false alarm coincidence probability does not take into account the case when candidate events are located on opposite sides of cell borders, edges and corners. In order to find these coincidences the entire cell coincidence grid is shifted by half a cell width in all possible $2^4 = 16$ combinations of the four parameter-space dimensions, and coincidences are searched in all 16 coincidence grids. This leads to a higher number of accidental coincidences, and consequently equation (A.4) underestimates the false alarm probability. Let us consider the simplest one-dimensional case. In this case we have $2^1 = 2$ possible shifts (the original coincidence grid and the one shifted by half). This increases probability $p_F\,(N_{\rm cell})$ by a factor of 2 if the two cell coincidence grids were independent. However the cells overlap by half and some coincidences would be counted twice. To account for this we divide the cells in the coincidence grid by half resulting in $2N_{\rm cell}$ cells and define the false alarm probability $p_F\,(2N_{\rm cell})$ that any given half of the coincidence cells out of the total of $2N_{\rm cell}$ half cells contains candidate events from $C_{\rm max}$ or more distinct data segments. These are coincidences that were already counted, and consequently the false alarm probability with the cell shift is $2p_F\,(N_{\rm cell}) - p_F\,(2N_{\rm cell})$. This results in the false alarm probability

$$P_F = 1 - \left(1 - \left(2p_F\left(N_{\rm cell}\right) - p_F\left(2N_{\rm cell}\right)\right)\right)^{N_{\rm cell}}. \tag{A.5}$$

To generalize the above formula to higher dimensions we need to consider further shifts and divisions of the cells. In the four dimension case this leads to the formula for the probability $P_F^{\rm shifts}$ that there are $C_{\rm max}$ or more independent coincidences in one or more of the $N_{\rm cell}$ cells in all 16 grid shifts given by

$$P_F^{\text{shifts}} = 1 - \Big[1 - \Big(2^4 p_F(N_c) - \Big(\tbinom{4}{1} p_F(2N_c) + \tbinom{4}{2} p_F\big(2^2 N_c\big) + \tbinom{4}{3} p_F\big(2^3 N_c\big) + \tbinom{4}{4} p_F\big(2^4 N_c\big) \Big) - \Big(\tbinom{4}{2} p_F\big(2^2 N_c\big) + \tbinom{4}{3} p_F\big(2^3 N_c\big) + \tbinom{4}{4} p_F\big(2^4 N_c\big) \Big) - \Big(\tbinom{4}{3} p_F\big(2^3 N_c\big) + \tbinom{4}{4} p_F\big(2^4 N_c\big) \Big) - \tbinom{4}{4} p_F\big(2^4 N_c\big) \Big) \Big]^{N_c}. \tag{A.6}$$

By choosing a certain false alarm probability P_F, we can calculate the threshold number $C_{\max}$ of coincidences. If we obtain more than $C_{\max}$ coincidences in our search we reject the null hypothesis that coincidences are accidental only at the significance level of P_F.

References

[1] Accadia T *et al* 2012 *JINST* **7** P03012
[2] Abbott B *et al* 2007 *Phys. Rev.* D **76** 082001
[3] Mastrano A, Lasky P D and Melatos A 2013 *Mon. Not. R. Astron. Soc.* **434** 1658
[4] Owen B J 2010 *Phys. Rev.* D **82** 104002
[5] Jones D J and Andersson N 2001 *Mon. Not. R. Astron. Soc.* **331** 203
[6] Bildsten L 1998 *Astrophys. J.* **501** L89
[7] Ushomirsky G, Cutler C and Bildsten L 2000 *Mon. Not. R. Astron. Soc.* **319** 902
[8] Cutler C 2002 *Phys. Rev.* D **66** 084025
[9] Melatos A and Payne D J B 2005 *Astrophys. J.* **623** 1044
[10] Owen B J 2005 *Phys. Rev. Lett.* **95** 211101
[11] Johnson-McDaniel N K and Owen B J 2013 *Phys. Rev.* D **88** 044004
[12] Brady P R, Creighton T, Cutler C and Schutz B F 1998 *Phys. Rev.* D **57** 2101
[13] Abbott B *et al* 2008 *Phys. Rev.* D **77** 022001
[14] Abbott B *et al* 2005 *Phys. Rev.* D **72** 102004
[15] Abbott B *et al* 2009 *Phys. Rev. Lett.* **102** 111102
[16] Abadie J *et al* 2012 *Phys. Rev.* D **85** 022001
[17] Jaranowski P, Królak A and Schutz B 1998 *Phys. Rev.* D **58** 063001
[18] http://einstein.phys.uwm.edu
[19] Abbott B *et al* 2009 *Phys. Rev.* D **79** 022001
[20] Abbott B *et al* 2009 *Phys. Rev.* D **80** 042003
[21] Aasi J *et al* 2013 *Phys. Rev.* D **87** 042001
[22] Acernese F *et al* 2008 *Class. Quantum Grav.* **25** 184001
[23] Accadia T *et al* 2010 *J. Phys.: Conf. Ser.* **228** 012015
[24] Astone P *et al* 2002 *Phys. Rev.* D **65** 022001
[25] Astone P, Borkowski K M, Jaranowski P and Królak A 2002 *Phys. Rev.* D **65** 042003
[26] Astone P, Borkowski K M, Jaranowski P, Piętka M and Królak A 2010 *Phys. Rev.* D **82** 022005
[27] Abbott B *et al* 2009 *Phys. Rev. Lett.* **102** 111102
[28] Schutz B F 1991 *The Detection of Gravitational Waves* ed D Blair (Cambridge: Cambridge University Press) pp 406–52
[29] Owen B 1996 *Phys. Rev.* D **53** 6749
[30] Conway J H and Slone N J A 1999 *Sphere Packings, Lattices and Groups* (New York: Springer)
[31] Prix R 2007 *Phys. Rev.* D **75** 023004
[32] Pletsch H J 2008 *Phys. Rev.* D **78** 102005